

Deflection behavior of focused-ion-beam deposited carbon nanocantilever and overhung structures

Prashant K Sarswat^{1,2*}, Madhusudan Jagannathan²

¹Department of Physics, Indian Institute of Technology Kanpur, Kanpur 208016, India

²Department of Metallurgical Engineering, University of Utah, Salt Lake City, UTAH 84112, United States

*Corresponding author, Tel: +1-801-520-6919; E-mail: saraswatp@gmail.com

Received: 25 July 2016, Revised: 28 August 2016 and Accepted: 30 October 2016

DOI: 10.5185/amlett.2017.6889

www.vbripress.com/aml

Abstract

Elastic properties of nanostructures are crucial for the adequate design and long term use of nano/micro-electro-mechanical system (NEMS/MEMS) as well as their utility in nanoindentation. Carbon nanostructures were fabricated by focused ion beam (FIB) assisted deposition and milling using Naphthalene (C₁₀H₈) as a precursor gas. Cantilevers of size 3-10 μm were fabricated and their elastic properties were monitored. An end point load was applied by successive deposition of Pt or carbon in a form of vertical column. Euler–Bernoulli beam theory was applied to examine the mechanical properties of the cantilever. It has been observed that expected deflection of the carbon nano-cantilever is significantly different compared to most of the reported micro or nano-sized carbon or diamond structures. Initial investigation of such a discrepancy suggests that Ga implantation and presence of core-shell type structure are the main causes of altered mechanical properties. Copyright © 2017 VBRI Press.

Keywords: Focused ion beam, CVD, MEMS, NEMS, cantilever.

Introduction

The focus areas of nanotechnology those are relevant for mankind and society are imaging, fabrication, healthcare, communication, consumer electronics, and sensing. Among these areas, nano-fabrication techniques are keys to miniaturization of electronic devices, biosensors, and devices used in defense technology [1-4]. Focused Ion Beam (FIB) technique has emerged as a powerful and unique way to rapidly build the prototypes of complex 3-D nanoarchitecture such as hanging beams, cantilevers, hollow and solid pyramids, plasmonic structures, and springs [5]. FIB technology provides unsurpassed opportunities of micro or nanoscale milling or deposition on the variety of substrates [1]. It has been reported that irradiation of ion beams on different substrates causes effects such as adhesion of thin film, scattering effects, sputtering of materials, and ripple formation [5]. For surface modifications, low energy ions (few keV) are useful whereas ion implantation is generally carried out using high energy ion (energy ~ few MeV) [5]. Hence, using appropriate energy and other deposition parameters, miniature nanostructures can be fabricated using the bottom-up approach [6]. FIB assisted fabrication offers advantages such as precise dimensional control and relatively less fabrication steps [7]. In this case step such as multistep photoresist etching process can be avoided.

Among nanostructures, miniature cantilevers are useful in applications such as near-field scanning optical microscopy (NSOM), biomolecule capturing, virus detection, electronic noses, femtogram, and quantum computing [8-10]. Microcantilever based actuator have been fabricated using polymer-metal combination [7]. Knowledge of cantilever material's elastic and mechanical properties helps to understand the performance, reliability, and durability of respective MEMS and NEMS sensing device when utilized repeatedly. In this regard, elastic properties of this class of devices have been investigated time to time. The spring constant of multiwalled carbon nanotube (MWNT)-mechanical piezo transducer was utilized to investigate mechanical properties [11]. It was calculated that such a nanotubes show spring constant of ~ 0.001 N/m and it is tunable in the range of ~ 0.001–0.05 N/m [11]. Similarly, amorphous carbon nanofiber (CNF) was grown on carbon-coated Si cantilever using argon ion bombardment [12]. Using Euler formula, Young modulus was determined by measuring buckling force. It had a value of ~ 38-48 GPa. Ishida *et al.* measured the spring constant and mechanical resonant frequency of amorphous carbon nanopillars fabricated using FIB [13]. It was concluded that the deposited material contains gallium which was evident in density excess [13]. Annealing of nanopillars helps to reduce the Ga content and density of nanopillar.

In this paper we will investigate the deflection behavior FIB-deposited cantilever structures. FIB system 'Nova 600 Nano Lab' used in this research was equipped with field emission Ga ion source, high resolution (7 nm) ion optics, high resolution milling and gas chemistry functionalities for deposition of C, Pt and W, e-beam patterning, scanning electron microscope (SEM) and energy dispersive spectroscopy (EDS). Carbon cantilevers of length in the range of 3- 10 μm and cross-sectional area 200 nm^2 to 5000 nm^2 have been fabricated using Ga ion beam. These cantilevers can be potentially useful for applications such as gap sensing devices, random-access memory elements, and NEMS switches [14]. Some other specific use of carbon material is a micromechanical system, data storage system, and field emission displays. Mechanical performance of the cantilevers such as stiffness, strain to failure, maximum stress, and Young's modulus can be evaluated by examining the bending behavior of a nanocantilever. For bending, various methods have been proposed and examined such as the use of the external device (AFM cantilever), light irradiation, and electrostatic interaction. However, we applied fixed point load by depositing the platinum or carbon pillars of variable height at the free end of the cantilever arm. The deflection profile of a cantilever was monitored before and after the loading. The value of Y turns out to be several orders of magnitude smaller than the bulk value. These results are presented and the discrepancy in the value was investigated.

Theory

Focused ion beam fundamentals

Most of the focused ion beam systems work on the principle of liquid metal ion source (LMIS) [5]. Nova 600 nanolabTM utilizes a reservoir of Ga^+ ions. For utility of Ga^+ ion beam, the temperature of a reservoir is raised up to point of evaporation. The heated Ga can be drawn by an annular extractor electrode that is concentric with the tip of the needle and closely located [1]. Ga can flow through a sharp, heat resistant needle tip that is linked to the reservoir and positioned close to an extractor. A high potential difference between aperture and needle creates an electric field $\sim 10^{10}$ V/m that is responsible for the acceleration of energetic ions towards extractor. Ion existence can be found in a region where the equilibrium between surface tension and electrostatic forces has drawn liquid Ga into a Taylor cone of apex size of ~ 5 nm. The small size of cone tip and intensity of extraction voltage is sufficient enough to pull Ga atom from needle tip and subsequent ionization by field evaporation [1]. After ionization, Ga^+ can easily accelerate by potential and maneuvered by the set of lenses, aperture, and alignment devices. Due to an intense electric field, there is a creation of 'tiny cusp' or 'incipient jet'. Once field evaporation allows ion emission to occur, ions start accelerating towards a downward side of the column. The 'extraction current' is the current that emits from the tip, it is regulated both by the extractor and the suppressor. The suppressor is useful to maintain constant

beam current. Its ability to maintain constant extraction voltage without source tip alteration is one of the important requirement of FIB system.

For deposition of carbon nano-structures, Naphthalene (C_{10}H_8) was utilized as a precursor gas. During digital mode scanning, Naphthalene interacts with the primary gallium beam to facilitate selective or preferred deposition of carbon structure by decomposing precursor gas molecules. The deposition proceeds with continuous adsorption of atoms on the substrate. The beam scanning is repeated until a desired thickness of structure has been achieved. The Z-direction growth is proportional to deposition rate, and hence height of the nanostructure can be controlled by varying beam irradiation time if deposition rate is fixed [15]. It should be noted that the ion beam has a greater effect compared to the electron beam, for the substrate in contact that causes removal of atoms beneath the target focus area, localized heating, and implantation of ions. Another point to understand is that gradual position scanning of a Ga ion beam during deposition causes the shifting of growth area around beam point [15]. Altogether, using FIB system the variety of complex nanostructures can be fabricated that can be useful for various NEMS applications (See Fig. 1).

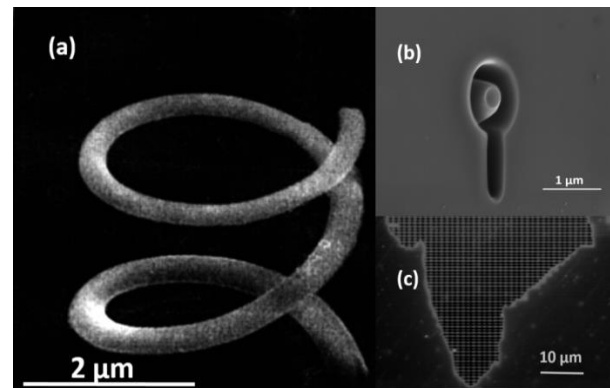


Fig. 1. Focused ion beam assisted fabrication of structures and pattern on Si: (a) Carbon nano-spring, (b) Key-type groove; and (c) A map made using Ga^+ assisted milling.

Deflection of cantilever

In civil engineering terminology, 'Cantilever' is a beam that is anchored at only one end (See Fig. 2a-b) [16]. The cantilevers are extremely useful for overhanging structures and bridges without external bracing [16]. In MEMS (microelectromechanical systems), cantilevers are generally made from silicon, silicon nitride or polymers.

There are two important equations that are utilized to explain cantilever bending behavior:

The Stoney equation relates the residual surface stress/length ($\Delta\sigma$) of a film to a curvature of the substrate (κ). It should be noted that curvature does not depend on geometric properties or type of materials. Such an equation, in original form, can be written as:

$$\kappa = \frac{6\Delta\sigma}{Et^2} \quad (1)$$

where, 't' is the thickness of the substrate and 'E' is elastic modulus. For long and wide cantilever plate, E can be replaced by the biaxial modulus $E/(1-\nu)$.

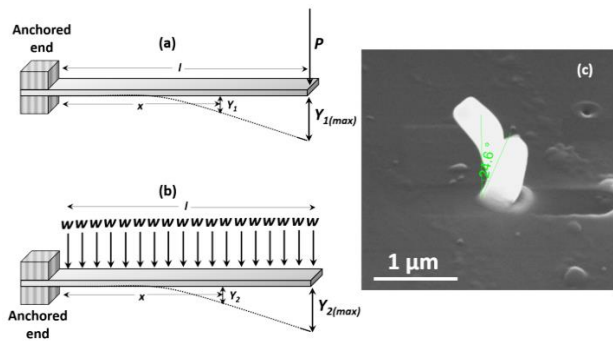


Fig. 2. Schematic diagrams of cantilever with load and deflection (a) End point load, (b) Uniformly load; and (c) Bending of Pt structure at bottom and joint. Such a bending causes difficulty in fabrication of overhanged structure.

In simple term, for concentrated load 'P' at one end, the deflection of beam at any point (located at distance 'x' from an anchored end) can be written as:

$$y_1 = \frac{Px^2}{6EI}(3l-x); \tag{2}$$

$$\text{Maximum deflection} = y_{1(\max)} = \frac{Pl^3}{3EI}; \tag{3}$$

For uniformly distributed load 'w (N/m)', the deflection can be written as:

$$y_2 = \frac{wx^2}{24EI}(x^2 + 6l^2 - 4lx); \tag{4}$$

$$y_{2(\max)} = \frac{wl^4}{8EI} \tag{5}$$

where, 'l' is the total length of a cantilever, 'I' is inertia of cantilever beam.

$$\text{Total deflection} = y_1 + y_2 \tag{6}$$

In case, concentrated load 'P' is acting at angle 'θ' from a perpendicular to beam. The deflection can be written as:

$$y_{1(\max),\theta} = \frac{Pl^3}{3EI} \cos\theta \tag{7}$$

Experimental

In this section method of nano-cantilever fabrication using FIB (FEI-Nova 600 nanolab™), will be explained. The resolution of an ion beam was ~ 7 nm. The minimum etched linewidth (for Si) was ~ 15 nm. In method 1, the cantilever was fabricated using a two-step method. First, a

cylindrical pillar was deposited on Si substrate. Subsequently an overhang arm was grown on side of cylinder at an end (we also conducted some test run; See Fig. 2c). In order to examine the deflection, carbon pillar was grown at the end of this overhang arm (See Fig. 3). All deposition experiments were conducted using 30 keV Ga ions with an ion current of ~ 30 pA. We first tried Platinum cantilever fabrication; however, it was observed that Pt cantilever structure was not much stable. It can be seen in Fig. 3 that cantilever structure starts bending from the bottom. After deposition of the side arm, the vertical pillar attains a permanent tilt of ~ 24° from vertical. Hence, carbon cantilevers were fabricated to examine their properties.

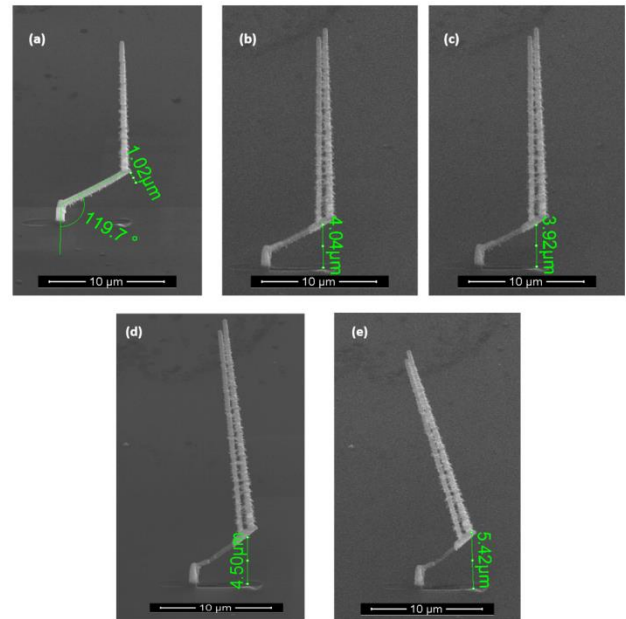


Fig. 3. Snapshots of cantilever bending after deposition of Pt end point load. Cantilever was fabricated using two step deposition method. First a cylindrical pillar was grown and secondly an arm was grown on top side of the pillar.

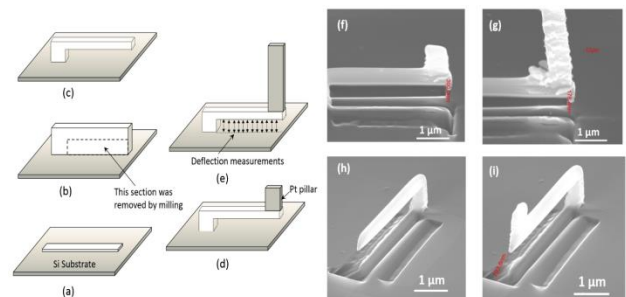


Fig. 4. (a-c). A schematic diagram, showing step by step method to fabricate cantilever using deposition of wall and subsequent milling of lower portion; for deflection of cantilever Pt pillar is deposited at end of overhanged arm (4d-4e); Side view (f-g) and 3D view (h-i) of cantilever before and after loading Pt pillar. A change in deflection can be seen before and after Pt loading.

In method 2, the carbon wall was deposited on Si substrate using FIB of 30 keV Ga ions at an ion current of ~ 30 pA. The height and length of the wall were ~ 500 nm and 4 μm, respectively. The thickness of wall was

~ 200 nm. Once desired height of the wall was achieved, a portion of the wall was removed to create a cantilever structure (See Fig. 4a-e for fabrication steps). For removal of the wall, ion beam milling was performed using 30 keV Ga-FIB. The final length of an overhanged beam was ~ 3.5 μm. The width and thickness of cantilever arm were ~ 500 nm and 250 nm, respectively. Fig. 4 (f-i) shows different SEM images of a cantilever. After fabrication of a cantilever, deflection profile of an overhanged portion was made using point to point measurements performed at high resolution. Afterward, deposition of a Pt pillar was done using methyl cyclopentadienyl trimethyl platinum (CH₃)₃Pt(CpCH₃) precursor gas with earlier discussed beam and ion current parameters.

Results and discussion

We first examined the cantilever grown by method 1. In this case, we systematically increased the height of pillar grown at the end and measured the distance between the datum and the cantilever hanging arm tip (See Fig. 3). An increased height will result in more and more load (due to the weight of deposited cylinder) at the end and can cause bending of the cantilever arm. There was a change of ~ 50 nm in cantilever deflection when a cylindrical arm of a height ~ 12 μm and diameter ~ 500 nm was grown. The height of pillar was continuously increased up to 17 μm. When it was not further possible to increase the height to increase load, mainly due to a beam shift and subsequent tilt of a cylindrical pillar, then another branch was grown adjacent to it. It was observed, there was the total deflection of ~ 150 nm in cantilever arm when another cylindrical branch of height ~ 17 μm (diameter ~ 400 nm) was deposited. Further increment in height caused an upward bending of the cantilever arm. It caused an anti-clockwise tilting of two long cylindrical branches and finally bending of the cantilever arm. These cylindrical arms were milled out to see if the cantilever can attain original geometry. However, there was a permanent deformation of a cantilever. Fig. 5(a) shows the experimental deflection profile of a cantilever.

It is interesting to observe that Young's Modulus value, obtained using two distinct experiments is not significantly different. We have simulated deflection profile of cantilever arm (loaded at the end) using Young's modulus value of ~ 100 GPa. It can be seen (see Fig. 5b) that simulated maximum deflection was ~ 1.7 × 10⁻¹³ m, which is very less compared to experimental value (See Fig. 5a). Such an observation was also consistent for cantilever without end point load. Additional simulations were performed using SolidWorks™ to predict the elastic displacement values for the nanocantilever structure. The structure was created as per the actual dimensions of the carbon cantilever. Three different values of the elastic modulus, 1.2 × 10¹¹ Pa, 6 × 10⁶ Pa, and 10⁴ Pa were plugged into the simulation to check how deflection varies with Young's Modulus. The load was imposed on the extreme edge of the beam with the base being fixed. The load value was

calculated from the mass of Platinum and the volume of the Pt pillar from experimental dimensions. The elastic displacement of the cantilever can be seen in Fig. 5 (c)-(e).

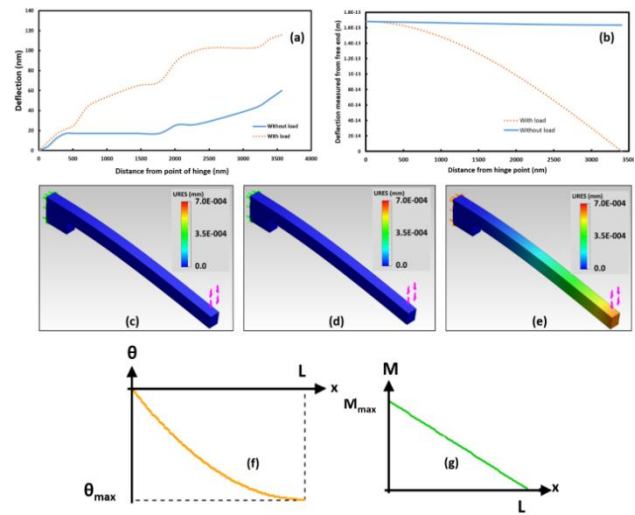


Fig. 5. Experimental (a) and (b) simulated cantilever arm deflection profile before and after loading. Elastic displacement simulation (in mm) in a geometry similar to the carbon wall nano-cantilever structure synthesized as per method 2 with elastic modulus values of (c) 1.2 × 10¹¹ Pa, (d) 6 × 10⁶ Pa, and (e) 10⁴ Pa, (f) Simulated slope profile and (g) moment profile of cantilever.

The displacement values in the legend are in mm. It can be seen that for Young's modulus of 1.2 × 10¹¹ Pa and 6 × 10⁶ Pa, the deflection in cantilever is much less than 10 nm whereas for the material with the elastic modulus of 10⁴ Pa, the deflection is in the range of 70 nm. This deflection value is nearest to the actually observed deflection in the C nano cantilever, thus indicating that the effective Young's modulus is nearer to 10⁴ Pa than 10⁶ Pa or higher.

The examinations of the deflection profile of a cantilever suggest that there were at least 2-3 locations where the sudden discontinuity in the deflection can be observed. It is important to mention that during simulation of the deflection profile no other phenomenon such as the effect of defects or dislocation was considered.

We have calculated a slope profile (Fig. 5f) and maximum slope using following equation:

$$\theta(x) = -\frac{P(2L-x)x}{2EI} \tag{8}$$

$$\theta_{\max} = -\frac{PL^2}{2EI} \tag{9}$$

Here 'θ' represents the slope. Using an estimated 'E' value, and other shape parameters, the maximum calculated slope is -4.92°.

Similarly, moment (M) and maximum bending stress can be calculated (See Fig. 5g):

$$M(x) = P(L - x) \quad (10)$$

$$M_{\max} = PL \quad (L \text{ is total length}) \quad (11)$$

Estimated maximum moment value, using equation (11) was $\sim 7.63 \times 10^{-19}$ N-m.

There are several causes that might be responsible for such an anomalous mechanical behavior. Among them, quality, crystallinity, and purity of deposited carbon are most important points to be discussed. It has been reported that ion beam assisted carbon is hydrogenated and amorphous [17]. Such a conclusion was made after Raman and nanoindentation examination. Raman examination of a carbon film and nanostructure show the broad and asymmetric peaks. In an examination, it was observed that the peaks were deconvoluted in G and D peak at ~ 1350 and 1550 cm^{-1} . These peak positions indicate the presence of amorphous carbon [17]. The range of Young modulus value was ~ 110 -125 GPa. The minimum Young's modulus was ~ 110 GPa, when FIB current was 3 nA. It was shown that the variation in Young's Modulus can be very large ~ 100 to 500 GPa, for amorphous carbon film [18]. Such a variation occurs, mainly due to the different fraction of sp^3 and sp^2 bonds [18]. In another report, atomic force microscopy assisted digital correlation method was applied to examine the mechanical and failure properties of hydrogen-free tetrahedral amorphous carbon (ta-C) MEMS structures [19]. For a specimen of size ~ 10 -50 $\mu\text{m} \times 1.5 \mu\text{m}$, Young's modulus was ~ 740 -780 GPa [19]. An investigation of FIB-deposited Platinum was carried out by Tao *et al*, it was concluded that at Ga ion energy ~ 32 keV, ion current ~ 80 pA, the deposited film composition was $\sim 46\%$ Pt, 24% C, 28% Ga, and 2% O [20]. Such a composition was examined using Auger analysis. Their examination also suggests that the deposited Platinum was amorphous [20].

The mechanical properties of FIB nanostructures greatly change due to Ga implantation caused by Ga^+ FIB irradiation [21]. Such an implantation causes non-uniformity and thus causes non-linearity in mechanical properties [21]. Diamond like carbon (DLC) and tungsten nanostructures were fabricated and Ga distribution/ion beam profile was measured. The Young's modulus distribution was also measured using resonance frequency method by utilizing e-beam irradiation. A nano-pillar of diameter ~ 100 nm was examined in atomic force microscope as well as in TEM, it was observed that Ga atoms are distributed throughout the pillar with the maximum concentration at center [21]. The absorbance of Ga in the center of the pillar was higher because mass absorption coefficient of Ga is higher compared to carbon. Such a condition results in the formation of core-shell type structure; here core can be understood as a Ga in center whereas carbon layer acts as a shell. In this situation, an accurate density of cantilever material cannot be predicted. Young's modulus distribution model in a DLC pillar was estimated using a Gaussian function. It was observed that Young's modulus ranged from 13.4

GPa to 375 GPa [21]. It was later concluded that analytical accuracy of multiple layer model was better compared to the single-uniform material model. Highly focused ion beam deposited nanostructures were investigated using SIMS analysis and Monte Carlo simulation [22]. Measurements revealed both lateral and vertical contamination caused by Ga^+ beam. It was concluded that during an application of dose $\sim 1 \times 10^{17} \text{ cm}^{-2}$, the surface concentration of $\sim 6 \times 10^{21} \text{ cm}^{-2}$ is possible [22]. It has been also concluded that even application of low FIB doses ~ 30 keV, $1 \times 10^{14} \text{ cm}^{-2}$, there was the generation of an amorphous layer of thickness ~ 50 nm.

It is important to mention while discussing Young's modulus and mechanical property that we have not considered the effect of plasticity and dislocations. Plastic deformation has a direct effect on alteration in stress field for grain subpopulation. Change in elastic properties was mainly explained on the basis of 'active slip system'. The exact role of Ga in our carbon cantilever is still not known, however, there is a great possibility of such active system presence in the cantilever. It may be asked cantilever deflection data probably obtained beyond yield point. However, unloaded cantilever also shows a similar estimated Young's modulus value in the order of $\sim 10^4$ Pa. It has been reported that pillar deformation resistance decreases after the linear response and is known as softening [23]. Such a softening depends on the pillar diameter and ratio of diameter to length [23]. Another interesting report discussed the formation of amorphous carbon filament of size ~ 10 nm or less during the fracture of amorphous carbon film due to nano-scale shear impact [24]. The report also revealed that such nanostructures formed after cyclic nanofatigue, have the significant degree of graphite ordering and presence of carbon onion [24].

Irradiation-induced manipulation of nanostructures is one of the most crucial points to discuss, for the possible explanation of an unusual mechanical property of carbon nanostructure. Irradiation-induced engineering in carbon provides several new dimension in research [25]. It includes merger or interconnection of nanostructure, production of 'carbon-onions' or even nucleation of diamond under certain condition. One of the exceptional ability of carbon-nanostructures [26] under irradiation is 're-organization' [25]. It is reported that energetic particle beam under certain condition created 'meta-stable' ohmic configuration that is away from equilibrium. Generation of an irradiation-induced anomaly in carbon nanosystem is different from bulk system, mainly due to the size limit of system [25]. There is a smaller probability of energy loss of colliding particle and such probability decreases with increasing electron or ion-energy. Due to miniature dimension, there is good chance that local temperature exceeds melting temperature. Severity can be understood by a fact that 30 eV energy when transferred to an isolated fullerene, can raise the temperature in fullerene up to 2000 K [25]. Some of the main irradiation induced defects are vacancies, adatoms, and dislocations. Some of the irradiation assisted effect enhances the properties of

nanotube while some are detrimental. Conducting tracks have been observed along the trajectory of ions after high energy irradiation of fullerene. There is a great tendency of irradiation-induced dangling bond saturation in carbon nanostructures, hence several new ways to engineer nanostructures, using e-beam is possible at high temperature. Self-contraction of carbon-onions [27] type nanostructures has been observed after several electron and ion beam irradiation. An irradiation induced heavy contraction of the carbon-onions have been observed and extent of pressure in the center of nano-structure is good enough for diamond crystal nucleation [25, 27]. Nanostructures under irradiation are generally not in a state of thermal equilibrium. There is a continuous generation of defects and heat release due to such an exposure. There is only a small fraction of transferred energy storage in persistent defects; energy flux through the crystals can fulfill the condition of self-organization. This discussion can be understood as there is great probability of 'unintentionally' defect creation in carbon based nanosystem due to an ion or e-beam irradiation. Specially, an effect of self-contraction phenomenon and treating our nano-cantilever as encapsulated materials (See Fig. 6) can explain bending behavior [25, 28, 29].

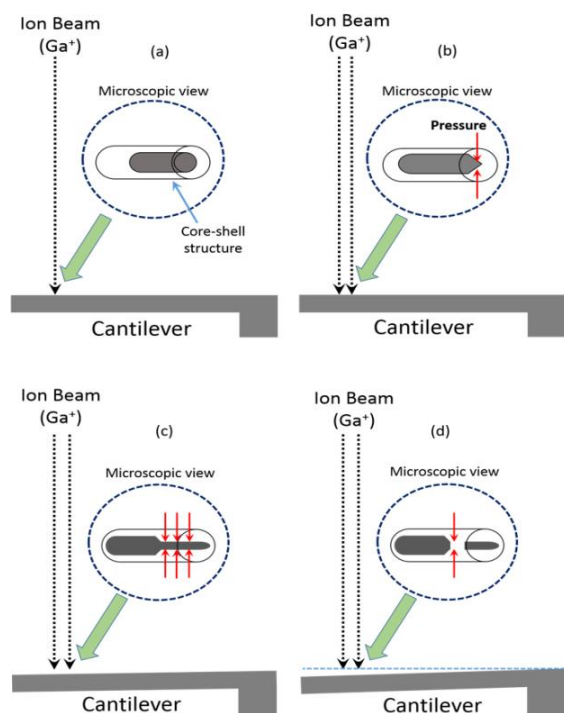


Fig. 6(a-d). A schematic diagram showing failure mechanism of carbon cantilever arm due to C-Ga core shell structure formation. Excess irradiation causes point pressure (see red arrows) on these cores that break apart due to extrusion of inner-shell material.

During beam irradiation, there is an extrusion of inner-shell material that will lead to the final collapse of nano-structure [25, 29]. Continuous extrusion and breakage can form slip plane that can cause easy movement or bending of the structure. Initially, this hypothesis was validated for a nanotubes-shell structure containing transition metals

(Fe, Co, or Ni) and later validated for relatively bigger dimension shell containing Ga [30]. A carbon pillar of thickness ~ 300 nm was fabricated and a high-angle annular dark-field transmission electron microscopy was performed [30]. It was observed that pillar has Ga-rich core. In order to understand nature of ion implantation in Ga-rich core we performed the simulation (see Fig. 7a-d) to predict range distribution and ion trajectory using SRIM 2008 software for 30 keV Ga ion in carbon [31]. For carbon layer, projected range is about ~ 22.8 nm and straggle is about ~ 57 Å. However for relatively low energy beam (10 keV) the projected range is about 10 nm and straggle is ~ 26 Å. Interestingly, when we considered two layers (one carbon ~ 30 nm and another containing 25% Ga ~ 30 nm) for simulation, both projected range, and straggle increased. It was further observed that when the thickness of the first layer reduces to ~ 20 nm straggle increases up to 73 Å. It suggests C-Ga core-shell type structures are more prone to ion interaction. Fig. 7e shows a systematic relationship between upper carbon layer thickness and straggle. Hence, in the background of this information, a possible excess bending mechanism of cantilever arm and effect of ion beam irradiation has been explained. Continuous irradiation due to successive deposition of long pillar causes more and more penetration of Ga and hence more chance of damage. There is a possibility to observe the effect of annealing, however, Ga-containing ZnO film shows a reduction in Young's Modulus after heat treatment [32].

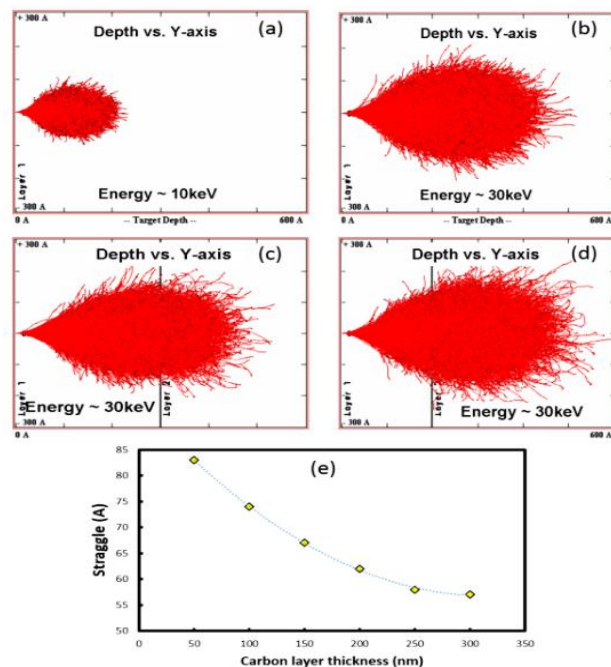


Fig. 7. Trajectory profile (Simulated using SRIM 2008) of Ga ion in carbon (a) Carbon layer of thickness ~ 60 nm, Ga^+ energy ~ 10 keV, (b) Carbon layer of thickness ~ 60 nm, Ga^+ energy ~ 30 keV, (c) Carbon layer of thickness ~ 30 nm, second layer contains 25% Ga and 30 nm thick; Ga^+ energy ~ 30 keV, (d) Carbon layer of thickness ~ 20 nm, second layer contains 25% Ga and 40 nm thick; Ga^+ energy ~ 30 keV; (e) Straggle vs. Carbon shell thickness relationship for 30 keV Ga ions, calculated using SRIM software.

Apart from the detrimental effect of Ga, unique properties of Ga-containing alloy in a context of FIB-deposited structures, is not fully explored [22, 33]. Hence it will be interesting to measure the beam deflection either by removal of Ga using low energy Ar ion nanomilling [34], or use of an in-situ annealing facility.

Conclusion

Deflection behaviour of miniature carbon cantilever arm, fabricated using focused ion beam deposition and milling, was studied. Deflection in overhanging cantilever arm was produced by depositing Pt pillar as an end point load. It has been observed that calculated elastic modulus value is significantly different compared to many of the reported value for DLC carbon. However, deposition parameter and purity of carbon nanostructure are not similar with most of the reported literature values. An anomaly in elastic property can be explained under the light of detrimental effect caused by Ga⁺ or e-beam irradiation. It is believed that successive irradiation can create self-contraction and extrusion that will lead to the collapse of nano-structure.

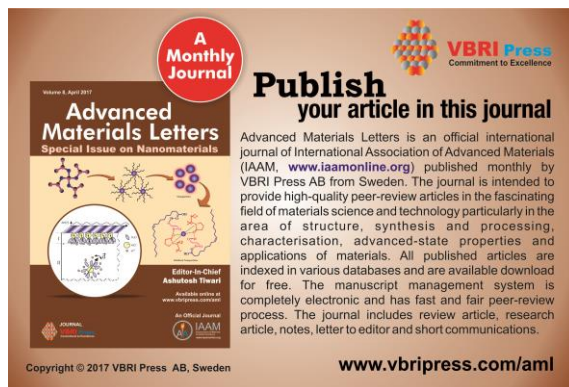
Acknowledgement

I am thankful to all staff members of Ion Beam Centre at IIT Kanpur, especially Mr. Sudhanshu Srivastava. I am also thankful to Late Prof. V. N. Kulkarni and Department of Science and Technology, India for technical discussion and financial support, respectively.

References

1. Yao, N. ed, *Cambridge University Press*, 2007.
2. Shukla, N.; Sarkar, M.; Banerji, N.; Gupta, A. K.; Verma, H. C.; *Carbon*, 2012, 50, 181.
DOI: [10.1016/j.carbon.2011.12.031](https://doi.org/10.1016/j.carbon.2011.12.031)
3. Sarswat, P. K.; Mishra, Y. K.; Free, M. L.; *Biosensors and Bioelectronics*, 2017, 89, 334.
DOI: [10.1016/j.bios.2016.07.019](https://doi.org/10.1016/j.bios.2016.07.019)
4. Bhattacharyya, D.; Sarswat, P. K.; Islam, M.; Kumar, G.; Misra, M.; Free, M. L.; *RSC Advances*, 2015, 5, 70361.
DOI: [10.1039/C5RA12191D](https://doi.org/10.1039/C5RA12191D)
5. Orloff, J.; Mark, U.; Lynwood, S., *Springer US: USA*, 2003; Vol. 1.
6. Srivastava, S.; Verma, K.; *Bulletin of Pure & Applied Sciences-Physics* 2013, (2).
7. Lee, C. C.; Alici, G.; Spinks, G. M.; Proust, G.; Cairney, J. M.; *Sensors and Actuators A: Physical*, 2011, 172, 462.
DOI: [10.1016/j.sna.2011.08.022](https://doi.org/10.1016/j.sna.2011.08.022)
8. Wang, Y.-H.; Lee, C.-Y.; Chiang, C.-M.; *Sensors*, 2007, 7, 2389.
DOI: [10.3390/s7102389](https://doi.org/10.3390/s7102389)
9. Jin, E. X.; Xu, X.; *Journal of Microscopy*, 2008, 229, 503.
DOI: [10.1111/j.1365-2818.2008.01935.x](https://doi.org/10.1111/j.1365-2818.2008.01935.x)
10. Li, M.; Tang, H. X.; Roukes, M. L.; *Nat Nano*, 2007, 2, 114.
DOI: [10.1038/nnano.2006.208](https://doi.org/10.1038/nnano.2006.208)
11. Ashutosh Tiwari, Y.K. Mishra, H. Kobayashi, A.P.F. Turner (Eds), *In the Intelligent Nanomaterials*, 2nd Edition, John Wiley & Sons, USA, 2016.
12. Inaba, K.; Saida, K.; Ghosh, P.; Matsubara, K.; Subramanian, M.; Hayashi, A.; Hayashi, Y.; Tanemura, M.; Kitazawa, M.; Ohta, R.; *Carbon*, 2011, 49, 4191.
DOI: [10.1016/j.carbon.2011.05.051](https://doi.org/10.1016/j.carbon.2011.05.051)
13. Ishida, M.; Fujita, J.-i.; Ochiai, Y.; *Journal of Vacuum Science & Technology B*, 2002, 20, 2784.
DOI: [10.1116/1.1526699](https://doi.org/10.1116/1.1526699)
14. Atul Tiwari, Ashutosh Tiwari (Eds), *Bioengineered Nanomaterials*, CRC Press, USA, 2013.

15. Matsui, S., Ed. *Springer Berlin Heidelberg*: 2010; Chapter 7, pp 211-229.
16. Timoshenko, S., *McGraw-Hill*: USA, 1953; p 452.
17. P. Lemoine, S. R., PD Maguire and JAD McLaughlin, *CRC Press*: USA, 2006; Vol. 3, p 4.
18. Schultrich, B.; Scheibe, H. J.; Grandremy, G.; Schneider, D.; *physica status solidi (a)* 1994, 145, 385.
DOI: [10.1002/pssa.2211450219](https://doi.org/10.1002/pssa.2211450219)
19. Cho, S.; Chasiotis, I.; Friedmann, T. A.; Sullivan, J. P.; *Journal of Micromechanics and Microengineering*, 2005, 15, 728.
DOI: [10.1088/0960-1317/15/4/009](https://doi.org/10.1088/0960-1317/15/4/009)
20. Tao, T.; Ro, J.; Melngailis, J.; Xue, Z.; Kaesz, H. D.; *Journal of Vacuum Science & Technology B*, 1990, 8, 1826.
DOI: [10.1116/1.585167](https://doi.org/10.1116/1.585167)
21. Shunjiro NISHI, R. K., Shinichi WARISAWA, Sunao ISHIHARA; *Journal of Advanced Mechanical Design, Systems, and Manufacturing*, 2010, 4, 7.
DOI: [10.1299/jamdsm.4.948](https://doi.org/10.1299/jamdsm.4.948)
22. Lehrer, C.; Frey, L.; Petersen, S.; Mizutani, M.; Takai, M.; Ryssel, H. In *Defects and gallium-contamination during focused ion beam micro machining*, Ion Implantation Technology, 2000. Conference on, 2000; pp 695-698.
23. Shibusani, Y.; Nakano, T.; Tanaka, H.; Kogo, Y.; *Journal of Materials Research* 2012, 27, 521.
DOI: [10.1557/jmr.2011.344](https://doi.org/10.1557/jmr.2011.344)
24. Wang, J. J.; Lockwood, A. J.; Peng, Y.; Xu, X.; Bobji, M. S.; Inkson, B. J., *Nanotechnology*, 2009, 20, 305703.
DOI: [10.1088/0957-4484/20/30/305703](https://doi.org/10.1088/0957-4484/20/30/305703)
25. Krashennnikov, A. V.; Banhart, F.; *Nat Mater*. 2007, 6, 723.
DOI: [10.1038/nmat1996](https://doi.org/10.1038/nmat1996)
26. Sarswat, P. K.; Free, M. L.; *Physical Chemistry Chemical Physics* 2015, 17, 27642.
DOI: [10.1039/C5CP04782J](https://doi.org/10.1039/C5CP04782J)
27. Banhart, F.; Ajayan, P. M.; *Nature* 1996, 382, 433.
DOI: [10.1038/382433a0](https://doi.org/10.1038/382433a0)
28. Sun, L.; Rodríguez-Manzo, J. A.; Banhart, F.; *Applied Physics Letters*, 2006, 89, 263104.
DOI: [10.1063/1.2403898](https://doi.org/10.1063/1.2403898)
29. Sun, L.; Banhart, F.; Krashennnikov, A. V.; Rodríguez-Manzo, J. A.; Terrones, M.; Ajayan, P. M.; *Science*, 2006, 312, 1199.
DOI: [10.1126/science.1124594](https://doi.org/10.1126/science.1124594)
30. Kometani, R.; Warisawa, S. i.; Ishihara, S.; *Japanese Journal of Applied Physics*, 2010, 49, 06GE03.
DOI: [10.1143/JJAP.49.06GE03](https://doi.org/10.1143/JJAP.49.06GE03)
31. Ziegler, J. F., SRIM-2003. Nuclear Instruments and Methods in Physics Research Section B: Beam Interactions with Materials and Atoms 2004, 219-220 (0), 1027-1036.
DOI: [10.1016/j.nimb.2004.01.208](https://doi.org/10.1016/j.nimb.2004.01.208)
32. Yamamoto, N.; Makino, H.; Yamamoto, T.; *Advances in Materials Science and Engineering* 2011, 2011, 10.
DOI: [10.1155/2011/136127](https://doi.org/10.1155/2011/136127)
33. Zhang, Y.-n.; Wu, R.-q.; Schurter, H. M.; Flatau, A. B.; *Journal of Applied Physics* 2010, 108, 023513.
DOI: [10.1063/1.3445269](https://doi.org/10.1063/1.3445269)
34. Unocic, K. A.; Mills, M. J.; Daehn, G. S.; *Journal of Microscopy* 2010, 240, 227.
DOI: [10.1111/j.1365-2818.2010.03401.x](https://doi.org/10.1111/j.1365-2818.2010.03401.x)



A Monthly Journal

Advanced Materials Letters
Special Issue on Nanomaterials

Volume 8, April 2017

Editor-in-Chief: Ashutosh Tiwari

Publish your article in this journal

Advanced Materials Letters is an official international journal of International Association of Advanced Materials (IAAM, www.iaamonline.org) published monthly by VBRI Press AB from Sweden. The journal is intended to provide high-quality peer-review articles in the fascinating field of materials science and technology particularly in the area of structure, synthesis and processing, characterisation, advanced-state properties and applications of materials. All published articles are indexed in various databases and are available download for free. The manuscript management system is completely electronic and has fast and fair peer-review process. The journal includes review article, research article, notes, letter to editor and short communications.

Copyright © 2017 VBRI Press AB, Sweden

www.vbripress.com/aml